Simple molecular model for ferroelectric nematic liquid crystals exhibited by small rodlike mesogens

N. V. Madhusudana [*]
Raman Research Institute, C.V. Raman Avenue, Bengaluru 560080, India

Nematic liquid crystals (NLCs) are the prime example of a liquid medium with an *apolar* orientational order. In the past couple of years, the *ferroelectric nematic* (FN) phase has been discovered in some compounds with small rodlike molecules with large longitudinal dipole moments and very *restricted* chemical structures, as the temperature is lowered from the NLC. We propose a simple model in which the molecules are idealized as cylindrical rods with *longitudinal surface charge density waves*. The usually strong electrostatic inter-rod interactions favoring antiparallel structures are shown to be subdued in magnitude, and those of parallel structures enhanced, by *reducing* the *amplitudes of the half-waves at both ends* of the rods. By introducing an additional increased amplitude of one interior wave, the energy per rod of a cluster of molecules with a pseudohexagonal order is shown to favor the ferroelectric order compared to the antiparallel order, below some value of the inter-rod separation. The model broadly accounts for the restriction in molecular structures for a compound to exhibit the FN phase. It is suggested that the *weakly first-order* nature of the NLC to FN transition arises from a coupling of the polar order and the density of the medium.

I. INTRODUCTION

Nematic liquid crystals (NLCs) are three-dimensional liquids with a spontaneous orientational order of the constituent organic molecules with anisotropy of shape [1]. The first molecular theory of orientational order was proposed by Born [2], who attributed it to intermolecular *dipolar* interactions between rodlike molecules. The isotropic (I) to nematic (N) phase transition would then correspond to a paraelectric to ferroelectric transition. The polarization (**P**) being a vectorial order parameter, the transition could be second order in nature. (Curiously, the first ferroelectric phase in a crystalline medium was identified several years later [3].) Onsager [4] subsequently showed that *excluded volume* interactions can stabilize orientational order in rodlike molecules, which gain translational entropy in the process. Maier and Saupe [5] demonstrated that *anisotropic dispersion* interactions lead to orientational order and could predict the NI transition temperature, which has a *weak first-order* character. Both of the latter models require the average orientation direction, represented by a unit vector **n** called the director, to be *apolar* in nature. The two theories have been combined to develop very realistic models of the nematic phase [6]. The apolar nature of **n** also means that the order parameter of the nematic is a second-rank tensor, which again leads to a weak first-order NI transition [1]. A direct proof of the apolar nature of **n** is the occurrence of ½ strength disclinations, which are line defects around which the **n**-field rotates by π radians, and they are the topological defects in the medium [1].

After the advent of liquid crystal displays (LCDs), a number of nematogens with strong longitudinal dipoles were synthesized to bring down the operating voltage [7]. Most of them had either the nitrile (CN) or nitro (NO$_2$) groups attached to one end of the aromatic core, and an alkyl or alkoxy chain with at least five or six carbon atoms at the other end to bring down the relevant transition temperatures. As the longitudinal component of the dipole moment in such a molecule is $\geqslant$5D, the dipolar interaction energy between neighboring molecules is significantly higher than $k_B T$, and as we argued [8], the favored mutual alignment is *antiparallel*. The liquid medium has antiparallel *short-range order* ensuring that **n** remains apolar. X-ray measurements on such compounds showed that the small-angle scattering corresponds to ~1.4 times the molecular length l [9], which also means that the strongest intermolecular energy corresponds to the dispersion interaction between the aromatic cores with high polarizabilities, and the chains of neighbors are on opposite sides, to form a partial bilayer structure [Fig. 1(a)]. The discovery of the reentrant nematic (N_{re}) phase below the temperature range of smectic A_d (SmA_d) phase with partial bilayer spacing both in mixtures [10] as well as pure compounds [11] made of strongly polar groups shows that the dipolar interactions are quite subtle. Compounds that exhibit the sequence I-N-SmA_d-N_{re}-SmA_1 have been synthesized [12], in which the layer spacing of the SmA_1 LC is equal to the molecular length l. Some polar compounds exhibit transitions between SmA liquid crystals with different layer spacings [13]. These unusual phenomena were accounted for by the phenomenological theory of two coupled order parameters developed by Prost [1]. The two order parameters correspond with the partial bilayer length ($>l$) and l itself. From a microscopic point of view, a frustrated spin gas model was developed to account for these phenomena [14],
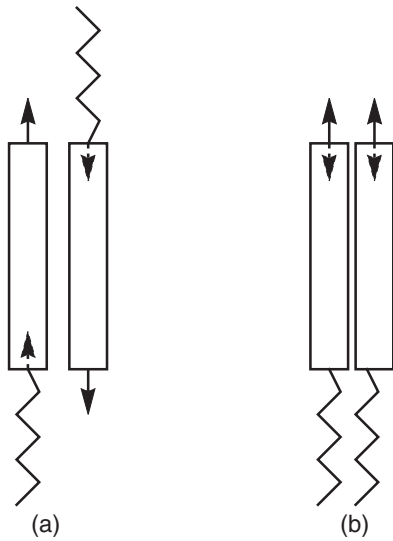
_____
[*]nvmadhu@rri.res.in

FIG. 1. (a) Schematic diagram showing the *antiparallel* alignment between two neighboring rodlike molecules with strong longitudinal dipoles which is favored at lower densities when the lateral distance between the molecules is large. The chains of the two molecules are far apart, generating the partial bilayer structure with a thickness $>l$, the molecular length. The dipole induced in a given molecule by the permanent dipole of the neighbor *increases* the net dipole moment. (b) When the separation between the molecules is decreased below some value, a parallel orientation with chains on the same side is favored. The net dipole moment is lower than the permanent dipole moment. The thickness of this structure equals l.

but the predicted transition temperatures and densities are too low [1]. As the $\mathrm{Sm}A_1$ phase occurs at temperatures *lower* than those at which the $\mathrm{Sm}A_d$ phase is stable, it is clear that the origin of $\mathrm{Sm}A_1$ is *not* due to a thermal dissociation of the partial bilayer structure made of antiparallel near neighbors.

In the antiparallel pair the two chains are far apart and have a negligible interaction [Fig. 1(a)]. If neighboring molecules have *parallel* orientation as in Fig. 1(b), the chains have a favorable dispersion interaction, though the dipoles now have positive electrostatic interaction energy. However, the polar end group of the neighbor now *induces* a dipole which is opposite in orientation to the given molecular dipole, thus reducing the effective dipole moment, and hence the repulsive energy. Both the dispersion interaction between the chains and the dipole-induced dipole interaction are $\propto r^{-6}$, where r is the lateral separation between the molecules, while the dipole-dipole interaction is $\propto r^{-3}$. Thus, as the density increases with a lowering of temperature, the parallel orientation can become more favorable [15]. The structure with parallel molecules has a lower McMillan parameter [1], and the medium with a sufficient concentration of the parallel species can no longer be in the smectic phase, thus giving rise to the N_{re} phase, which goes over to the $\mathrm{Sm}A_1$ phase at a lower temperature. Interestingly, in favorable cases, there can be a jump in the relative concentration of the parallel and antiparallel structures at some temperature, giving rise to a nematic to nematic (NN) transition [16]. The ferroelectric order corresponding to the parallel structure is *short-ranged* in view of the unfavorable dipolar energy, and the macroscopic symmetry of the nematic is again characterized by the apolar director **n**. The NN transition is

thus weakly first-order in nature, and it has been observed both in a binary mixture [17] and a single-component highly polar compound [18]. Dielectric studies on the latter compound at *high* electric fields ($\sim 10\,\mathrm{V}/\mu\mathrm{m}$) clearly demonstrated that ferroelectric short-range order grows with the field, and even gives rise to a measurable second-harmonic current signal at very high fields [19].

There is in principle nothing against a nematic liquid crystal exhibiting a spontaneous *ferroelectric long-range order* with polarization **P** as originally proposed by Born [2]. There have been several theoretical studies and computer simulations exploring this possibility. Practically all of them assume that a strong *point dipole* is located usually at the center of the molecule. A succinct review of the earlier theoretical work is given in Ref. [20]. Thus, Monte Carlo simulations of polar hard spheres [21], and molecular dynamic simulations of polar soft spheres [22], showed that the electrostatic interactions lead to the formation of chains at low densities and ferroelectric long-range order at relatively high densities, depending on the strength of the point dipole. MC simulations of hard spherocylinders with strong longitudinal dipoles were shown to exhibit antiparallel orientation of nearest neighbors as expected, with both positional and orientational correlations being short-ranged [23]. Interestingly, with a *transverse orientation* of dipoles the rods could form monolayer smectic structure, with a hint of ferroelectric order in the plane of the layer [23]. A numerical calculation based on the Onsager formalism for excluded volume interactions between hard spherocylinders, and including an *effective* potential that *favors* parallel orientation of longitudinal dipoles, was used to find ferroelectric order in the nematic beyond a threshold value of dipolar strength [24]. Depending on the parameters, the sequence *isotropic-apolar nematic-ferronematic* was found as the *density* was increased. However, an earlier study [25], in which a *coupling* of the nematic and polar orders was taken into account, had shown that only dipolar *disks*, which can form chains, rather than rods, formed the ferroelectric phase as the temperature was lowered from the nematic. A formal density functional theory has been proposed [26] in which the free energy of a polarized medium is split into a short-ranged part and a long-ranged electrostatic part that depends on the shape of the sample and the electrical boundary conditions. The anisotropic electrostatic interactions between the dipolar spheres leads to the formation of chains, and the authors found that the interaction between such chains can form the ferroelectric phase (as found in polar polymers; see the next paragraph) at densities comparable to those found in simulations, though in the latter, there was no evidence of chains in the ferroelectric phase itself [26]. If the dipolar spheres form a *uniformly* polarized medium, the long-ranged dipolar interaction between a given location and that in a spherical shell around it is identically zero [20]. This means that in the mean-field approximation, the long-range dipolar contribution is negligible, and the *dipolar interaction becomes effectively short-ranged*, significant only over the correlation length. A detailed analysis of short-range steric interactions between slightly nonspherical molecules with point dipoles that are aligned at an angle to the symmetry axis again confirmed that disklike particles are better suited for the appearance of a ferroelectric nematic that has uniaxial symmetry

[20]. As was already noted in Ref. [25], the dipolar interaction between a dipole and another *parallel* dipole, which is *free to move in a line* that is oriented parallel to the dipole, but does not contain the first dipole, *averages out to zero*. If the second dipole moves in a line containing the first, the *average* negative electrostatic interaction energy just depends on the length of the molecule. Thus, even if the polar molecules have strong deviations from spherical symmetry, in the resulting ferroelectric medium with a cylindrically symmetric distribution function, the *effective dipolar interaction is short-ranged*. In short, the statistical theories that have been developed for nematics made of small molecules with point dipoles predict the occurrence of the ferronematic nematic (FN) phase if the molecules are either spherical or disk-shaped [20,25,26], and the dipolar interaction is essentially short-ranged. If the molecules are rod-shaped, a short-ranged antiparallel alignment is to be expected [8,23], and a ferroelectric order results only if a *favorable effective potential* is assumed, whose origin has *not* been worked out on the basis of dipolar interactions [24].

Experimentally, two systems were found some time ago in which proper ferroelectricity results from electrostatic interactions. If monomers with longitudinal dipoles are used to synthesize polymers, the *net dipole moment* of a polymer chain can be extremely *large*, and the possibility of polar organization becomes very favorable [27]. Indeed, optical SHG studies have been used to identify the *ferroelectric nematic* phase in a few different polymeric systems [28], but only when at least ∼30 monomers are joined to form the polymer. The rotational viscosity of these polymers is quite large, and they cannot be used in any application in which fast switching is required. In fact, the familiar switching technique has not been used to measure the polarization **P** of these systems.

The Sm*AP* liquid crystals are made of bent core (BC) molecules with relatively large opening angles (∼140°), in which the smectic *A* layers exhibit transverse polarization in the plane of the layers. Successive layers can have either an antiferroelectric [29] or a ferroelectric [30] order. Thus, each layer can be treated as a two-dimensional (2D) system, in which isotropic to 2D-nematic to 2D-ferronematic phase transition can take place. Though the bent shape of the molecules can help in the polar packing of the BC molecules, it has been argued that the electrostatic interactions between the molecules are more significant, and the Sm*AP* is a proper ferroelectric [31]. As the total interaction energy between a given dipole and those with a parallel orientation lying on a circle around the former is nonzero, it has been argued that the dipolar energy is long-ranged in the 2D case [31]. However, as noted earlier, the energy between a dipole and another which freely translates along a parallel line is zero, and even in the 2D case the dipolar interaction is short-ranged, occurring mainly between the near-neighbor BC molecules along the polar direction.

Remarkably, two compounds with *small* highly *polar rod-like* molecules were found to exhibit nematic to nematic transitions in 2017 [32–34]. The chemical structures of the two molecules are shown in Fig. 2. The compound shown in Fig. 2(b) with $R_1 = H$ and $R_2 = F$, with a molecular dipole moment of 9.43D, was found to have three nematic phases [34] exhibiting the following transitions on cooling:
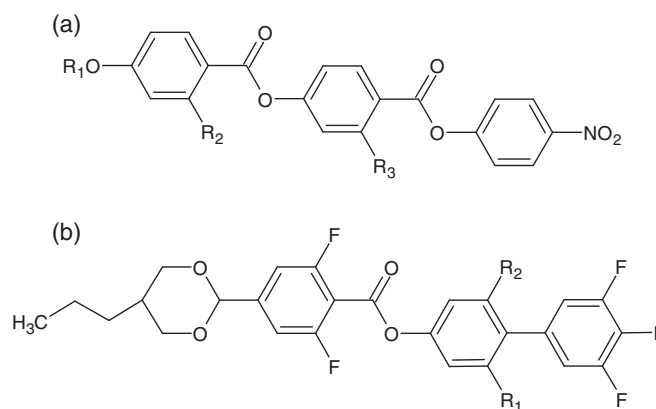

FIG. 2. General structural formulas of the molecules that exhibit the ferroelectric nematic phase. Note that both the polar NO_2 and the *three end* F substitutions give rise to a reduced effective lateral charges. The chain lengths at the other end are also short in the compounds exhibiting the ferroelectric nematic (FN) phase.

M1 84.5 °C M2 68.8 °C MP, both transitions being weakly first-order, though the M2 to MP transition is considerably stronger. Further, in a planar cell, *visible flow* occurs at the latter transition, implying *considerable rearrangement of the molecules*. Detailed dielectric, polarization switching and optical SHG studies were used by the authors to conclude that M1 is the usual NLC, and M2 a paraelectric phase. $\varepsilon_\parallel$, the low-frequency dielectric constant parallel to the director, jumped to ∼9000 as the sample was cooled across the transition from M2 to MP phase, in which it increased to ∼11 000 at lower temperatures. Further, the switching current measurements showed that in the MP phase, the sample exhibited a hysteresis loop, with polarization ranging between 3.5 and 4.4 $\mu C/cm^2$, depending on the temperature. The optical SHG signal had a nonzero value in the *absence* of external *electric field* **E**, the signal increasing by about six times when an external field **E** = 0.6 V/μm was applied. All these phenomena are consistent with the MP phase being a *ferroelectric*. If the dioxane ring with two oxygen atoms [see Fig. 2(b)] is replaced by an oxane ring with just *one oxygen* atom, the low-temperature phase is *not* exhibited [34]. X-ray studies showed that the medium has no positional order in the MP phase, exhibiting only a diffuse diffraction maximum corresponding to the molecular length l.

The compounds with the nitro end group [Fig. 2(a)] with $R_3 = H$, R_1 being either CH_3 or C_2H_5, and R_2 being OCH_3 or OC_2H_5 or OC_3H_7, exhibited a nematic-to-nematic transition. X-ray scattering studies on an oriented sample unusually showed *diffuse* maxima up to *three orders* corresponding to the molecular length l in both of the nematic phases. Curiously, if NO_2 is *replaced* by CN, or if R_2 is *shifted* to the *ortho* position on the phenyl ring, or replaced by H, the transition *disappears* [32,33]. Later light scattering measurements of the elastic constants of the compound named RM734, with $R_1 = CH_3$, $R_3 = H$, and $R_2 = OCH_3$, show that the splay elastic constant (k_{11}) starts to decrease rapidly at ∼ $T_{NN} + 4$ K, reaching nearly 0 as the temperature approaches $T_{NN} = 133$ °C, from the higher-temperature nematic phase [35]. Second harmonic (SH) microscopy shows a structure

with a periodicity of $\sim$4 to 5 μm. The authors of [35,36] identified the lower-temperature N phase as a splay nematic phase, and they proposed a model in which a coupling between the flexoelectric polarization and the splay distortion of the nematic leads to a softening of k_{11}, as in an earlier model of the nematic phase made of bent core molecules [37]. In the splay nematic phase, alternate splayed structures have an antiferroelectric alignment [35,36]. More recent investigations by the Boulder group [38] have clearly established that the lower-temperature *nematic* is a *ferroelectric* phase, with the polarization **P** increasing to $>6 \, \mu$C/cm^2 at low temperatures ($\sim T_{NN} - 40$ °C), which is close to the value expected from a fully aligned sample with $\langle P_1(\cos\theta)\rangle \approx 1$, where θ is the angle made by the long axis component of the molecular dipole moment (≈ 11 D) with **P**. A splay deformation of **P** would induce charge densities that give rise to a large *positive* energy, and the spatial variations in the orientation of **P** in the ferroelectric nematic (FN) take place preferentially by twist and bend deformations [38]. When a uniformly oriented thin ($\sim$2 μm) planar sample is cooled across T_{NN}, domains with opposite orientations of **P** can be seen, and a dc electric field applied in a direction opposite to **P** starts to reorient the latter beyond a Freedericksz threshold of $\sim$1 V/cm, which is about 1000 times smaller than that needed in the usual nematic phase with an apolar **n**. The authors also conducted MD simulations with both polar and apolar orientations of the molecules to find energy minima with the *anisotropic* radial distribution functions pointing to a few *preferential* relative positions of neighboring molecules in both cases [38]. Recently, MD simulations have been made in systems of both RM734 and RM734-CN molecules, with the NO$_2$ end group of the former replaced by CN in the latter [39]. The *dipole moments* of the two molecules are essentially the *same*, but the cyano compound does *not* exhibit the ferroelectric phase. The simulations showed that compared to the apolar structure, the polar structure has a lower energy of $\sim$2.2 kJ/mol in RM734 and only $\sim$0.14 kJ/mol in RM734-CN. The absence of the FN phase in RM734-CN shows that a *large* longitudinal molecular *dipole moment* is by itself *not a sufficient condition* for the occurrence of the FN phase.

Very recently, several new compounds with small variations in the structures shown in Figs. 2(a) and 2(b) have been synthesized [40], and measurements of the dielectric properties have shown that 17 of them have $\varepsilon_\parallel > 6500$, and all of them also exhibit SHG signals at low temperatures, implying that they are ferroelectric. In the structure shown in Fig. 2(a), compounds with $R_1 = $ CH$_3$, $R_2 = $ H, and $R_3 = $ OCH$_3$, OC$_2$H$_5$, and OC$_3$H$_7$ exhibit the ferroelectric phase if the end group is NO$_2$ but *not* if it is CN. With some compounds in which the NO$_2$ group of the end phenyl ring of Fig. 2(a) is replaced by the three F atoms in ortho positions as in Fig. 2(b), the *ferroelectric* nematic is *retained* in the altered compounds [40]. The authors note that in *all* the cases, (i) the FN phase occurs as the sample is cooled from the apolar N phase, (ii) both the dielectric constant and SHG signal start to increase at $\sim$15 K above the transition point, (iii) stripes are seen in unrubbed planar samples, which are identified as splay stripes, and they are not seen in rubbed planar samples due to strong surface anchoring, and (iv) a periodic filamentary texture is seen in the FN phase [34,40].

The authors have also used a machine learning software to analyze their data on both compounds, which exhibit as well as those that do not exhibit ferroelectric nematic to identify some molecular parameters that distinguish between the two types. The compounds exhibiting the ferroelectric nematic satisfy the following criteria: (i) the dipole moment of the molecule is $\geqslant$9D, (ii) the molecular length-to-width ratio is $\lesssim$2.5, (iii) the dipole moment of the molecule makes an angle between $\sim$10° and $\sim$25° with the long axis, and (iv) the length of the molecule itself is between $\sim$20.5 and 22 Å, which is a particularly narrow range.

We can note the following features found in *all* the variants which have been found to exhibit the ferroelectric nematic phase: (i) At one *end* of the molecule, the dipolar group has *lateral components*, as can be seen in Figs. 2(a) and 2(b). If there is no lateral component, as in the case of, say, the CN end group, the compound does not exhibit the ferrophase. (ii) At the other end, the *chain* should be *short*, with not more than three carbon atoms. (iii) The molecules have three phenyl rings with either ester linkage groups or fluorine substituents, which also have lateral components of dipole moments. (iv) The nematic phase which separates from the isotropic phase is the usual type found, say, in compounds such as cyanobiphenyls, with an antiferroelectric short-range order. (v) The ferroelectric phase occurs at lower temperatures, in which the *density* is *higher*, and hence the intermolecular separation is smaller. Using these features, in the following section we propose an idealized model for the structure of the polar molecules, and we show that the intermolecular electrostatic interactions favor the antiparallel organization at larger lateral intermolecular separations (R_0), and the parallel (polar) organization as R_0 is reduced below some value.

II. AN IDEALIZED MODEL OF POLAR MOLECULES

Our interest is to look for *general features* of the molecules that can form the ferroelectric phase, and the experimental systems have fairly rigid molecules with very short chains only at one end. The molecules can be expected to *freely rotate* about their *long axes* in nematic liquid crystals. A circular cylindrical rod of length $l = 22$ Å reflects a typical molecule of the compounds exhibiting the ferroelectric phase [40]. The diameter is typically about 4.5 Å, but more importantly, we make the following assumption about the idealized *polar* structure, which is relevant for our problem. The molecules shown in Figs. 2(a) and 2(b) have dipolar groups with lateral components attached to the highly polarizable phenyl rings. This feature results in alternating positive and negative charge densities along the length of the molecule (see, for example, Fig. S20 in the supplementary information of Ref. [38]). The molecules freely rotate about their long axes in the nematic phase. We assume that the molecular polar structure can be represented by *four surface charge density waves* along the length of the cylinder, of equal wavelength $\lambda = l/4$ and located on the surface at a radius $r = 2$ Å from the axis of the cylinder. The areal charge density is assumed to have sinusoidal variation along the length, but the *amplitudes* in neighboring *half-waves* need not be equal, though the total charge of the molecule should add to 0. The amplitudes
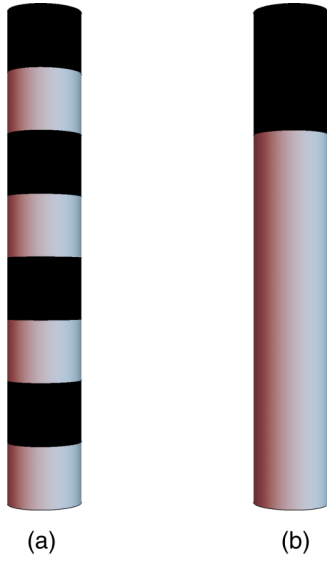
FIG. 3. Schematic figures showing the proposed idealized models of the polar molecules. As shown in (a), the structure has four surface charge density waves of equal wavelength along the length (Z) of the cylindrical rod. The parts with a lighter shade have positive charges, and those with a darker shade have negative charges. The charge density has a sinusoidal variation along Z, though the amplitude of each half-wave can be different. The amplitudes are given by s1 for the bottommost half-wave starting at $Z = 0$ (with positive charges), s2 for the next half-wave (with negative charges), etc. It is clear that the rod has a net longitudinal dipole moment, and for the sake of simplicity we use the *symbol* shown in (b) in some later figures to *represent* the polar rods, the smaller section with a darker shade at the top representing the arrowhead of the polar molecule.

FIG. 4. Schematic diagram showing the polar coordinates corresponding to the point a1 on the charged surface of rod 1 and a2 on rod 2. R_0 is the distance between the axes of the two rods. The shift along the length (Z-axis) between the two rods is $\zeta(21)$. The azimuthal angles of the two points on the two rods with respect to the X axis are $\varphi 1$ and $\varphi 2$, and their vertical shifts from the bottom surfaces of the respective rods are Z1 and Z2.

of the successive half-waves starting at $Z = 0$ are denoted by s1, s2, …, s7, and s8, respectively [Fig. 3(a)], i.e., the charge density $\sigma(Z)$ varies as $s1 \sin(2\pi Z/\lambda)$ between $Z = 0$ and $\lambda/2$, $s2 \sin(2\pi Z/\lambda)$ between $Z = \lambda/2$ and λ, etc., and finally $s8 \sin(2\pi Z/\lambda)$ between $Z = 7\lambda/2$ and $Z = 4\lambda = l$. As we assume that all amplitudes si have positive sign, the first half-wave along the rod is positively charged, etc., and the last half-wave is negatively charged [Fig. 3(a)]. This charge distribution also results in a large longitudinal dipole moment for the rod as a whole. Our main interest is to calculate the energy of a collection of such rods which can have an apolar or polar order. We first calculate the energy of a *pair* of parallel or antiparallel rods.

The axes of the two rods labeled 1 and 2 are assumed to be parallel to the Z-axis, and they lie in the XZ plane (Fig. 4),

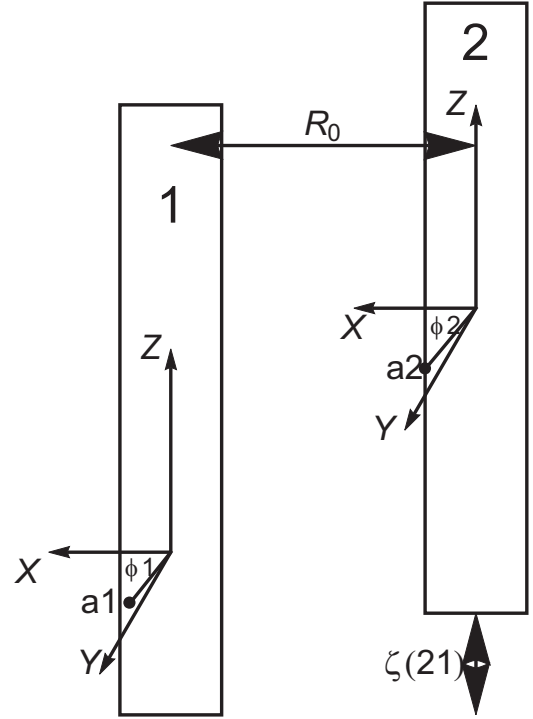with a separation of R_0 along X. The bottom edge of rod 1 corresponds to $Z = 0$ of the space fixed coordinate system XYZ. We also assume that the lowest half wave of rod 1 corresponds to s1 defined earlier. If rod 2 is parallel to rod 1, the bottommost half-wave of that rod also corresponds to s1. If the two rods are antiparallel, the bottommost half-wave of rod 2 corresponds to s8. The rod 2 is shifted by $\zeta(21)$ along Z with respect to rod 1. The locations of points a1 in the charged surface of rod 1 and a2 in the charged surface of rod 2 are described by Z1 and Z2 measured along Z from the bottom surface of the given rod, and the azimuthal angles $\varphi 1$ and $\varphi 2$ from the X axis, measured in the XY plane (Fig. 4). The distance between a1 and a2 is given by

$$d12 = \sqrt{(R_0 + r\cos\varphi 2 - r\cos\varphi 1)^2 + r^2(\sin\varphi 2 - \sin\varphi 1)^2 + [\zeta(21) + Z2 - Z1]^2}, \tag{1}$$

where r is the radius of the cylinder. If a1 is in the ith half-wave of rod 1, and a2 the jth half-wave of rod 2, the electrostatic interaction energy between the two *half-waves* for *parallel* rods is given by

$$e_P(i,j) = \frac{1}{4\pi\varepsilon_0} \int_0^{2\pi} rd\varphi 1 \int_0^{2\pi} rd\varphi 2 \int_{\frac{(i-1)\lambda}{2}}^{\frac{i\lambda}{2}} si \sin\left(\frac{2\pi Z1}{\lambda}\right) dZ1 \int_{\frac{(j-1)\lambda}{2}}^{\frac{j\lambda}{2}} sj \sin\left(\frac{2\pi Z2}{\lambda}\right) dZ2 \frac{1}{d12(Z1, Z2, \varphi 1, \varphi 2)}. \tag{2}$$
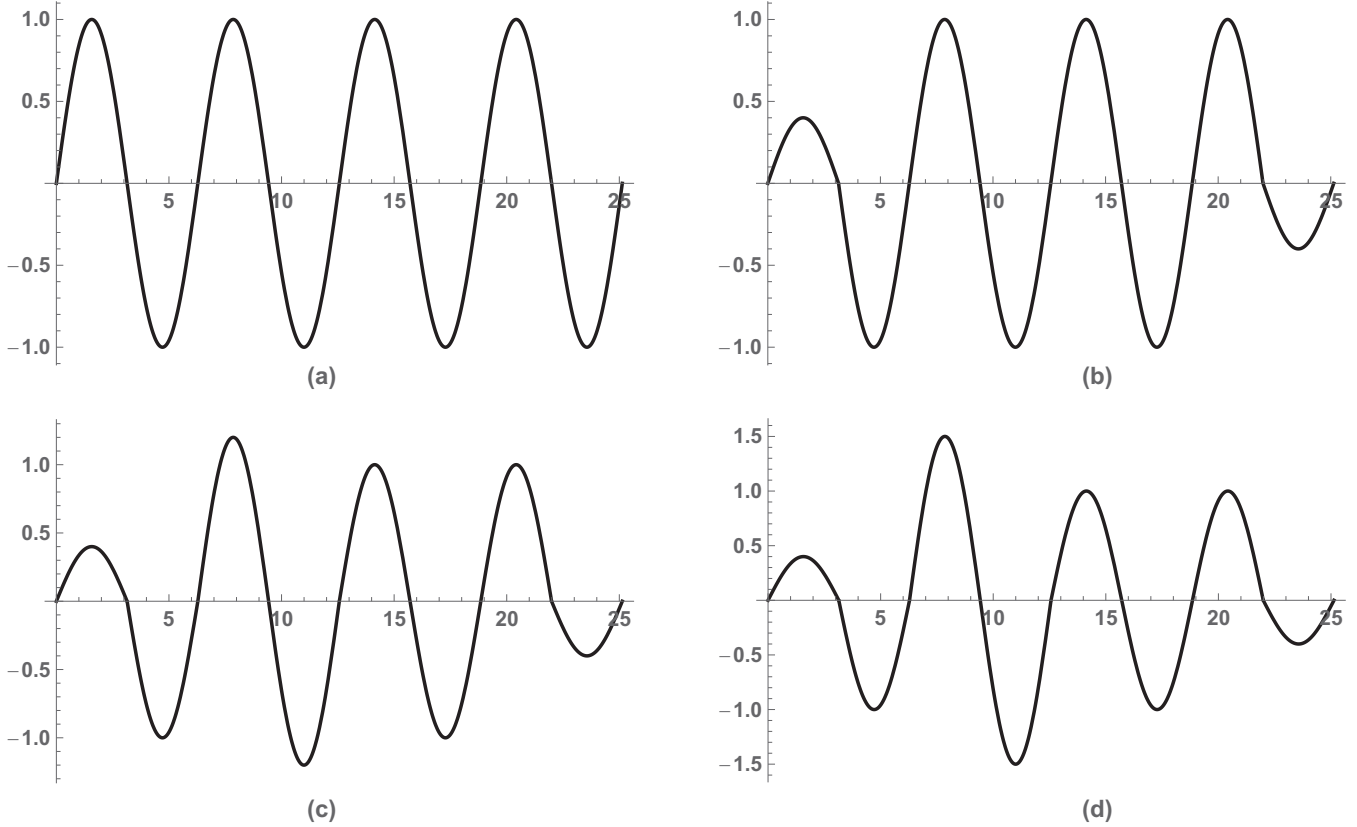
FIG. 5. Sinusoidal variation of the charge densities along the length of the rod in the four cases described in the text. The variations are shown for $l = 25$ Å in the illustrative diagrams, but as most compounds exhibiting the FN phase have $l \approx 22$ Å [40], all calculations of the energies have been done for $l = 22$ Å.

If the two rods are *antiparallel*, the energy is given by

$$
e_{AP}(i, j) = \frac{1}{4\pi\varepsilon_0} \int_0^{2\pi} r d\varphi 1 \int_0^{2\pi} r d\varphi 2 \int_{\frac{(i-1)\lambda}{2}}^{\frac{i\lambda}{2}} si \sin\left(\frac{2\pi Z1}{\lambda}\right) dZ1
$$

$$
\times \int_{\frac{(j-1)\lambda}{2}}^{\frac{j\lambda}{2}} s(9-j) \sin\left(-\frac{2\pi Z2}{\lambda}\right) dZ2
$$

$$
\times \frac{1}{d12(Z1, Z2, \varphi1, \varphi2)}. \tag{3}
$$

The total electrostatic energy between the two rods is

$$
E(R_0, \zeta(21)) = \sum_{i,j=1}^{8} e(i, j). \tag{4}
$$

Many purely geometrical parts of the integrals in Eqs. (2) and (3) are identical, reducing the number of calculations needed.

In the following, we present results on four combinations of the amplitudes si, with i varying from 1 to 8.

Case A: All amplitudes are equal, and assumed to be equal to 1 [$s1 = \cdots \cdots s8 = 1$; see Fig. 5(a)].

Case B: $s1 = s8 = 0.4$, $s2 = \cdots \cdots s7 = 1.0$, i.e., the amplitudes of only the first and last half-waves are lowered [Fig. 5(b)].

Case C: $s1 = s8 = 0.4$, $s3 = s4 = 1.2$, all other amplitudes are equal to 1 [Fig. 5(c)].

Case D: $s1 = s8 = 0.4$, $s3 = s4 = 1.5$, all other amplitudes are equal to 1 [Fig. 5(d)].

The Z-dependences of the charge densities in the four cases are shown in Fig. 5. We can now calculate the electrostatic energy of interaction between two parallel and antiparallel rods as functions of the relative shift in their positions $\zeta(21)$, for given values of R_0. As the ferroelectric nematic is the low-temperature phase, with small intermolecular separations, we first assume $R_0 = 4.6$ Å. In all four cases, $s2 = s5 = s6 = s7 = 1$ is the relative *reference* amplitude. If the corresponding physical amplitude is σ Coulomb/m^2, all the energy values shown in arbitrary units in Figs. 6, 8, 9, and 10 should be multiplied by $7.19 \times 10^{-20} \sigma^2$ to convert them to Joules. This can be compared with a typical thermal energy $k_B T \approx (5–6) \times 10^{-21}$ J.

Results for the parallel and antiparallel rods are shown in Figs. 6(a) and 6(b), respectively. The calculations have been made from $\zeta(21) = -l$ to $+l$. We note the following points: (i) As expected, unlike in the antiparallel case, in the parallel case the energy does not depend on the sign of $\zeta(21)$. (ii) Again as expected, the energy exhibits minima when the positively charged half-waves of rod 1 are in register with the negatively charged half-waves of rod 2 and vice versa. (iii) When all the amplitudes s1 to s8 are *equal* (case A), the deepest minimum energy of $\sim$−16 units occurs for the AP structure with $\zeta(21) = 0$, while the lowest minimum for the P structure is only $\sim$ −4 units for $\zeta(21) \approx \lambda/2$. It is clear that in this case, the ferroelectric structure cannot form. (iv)
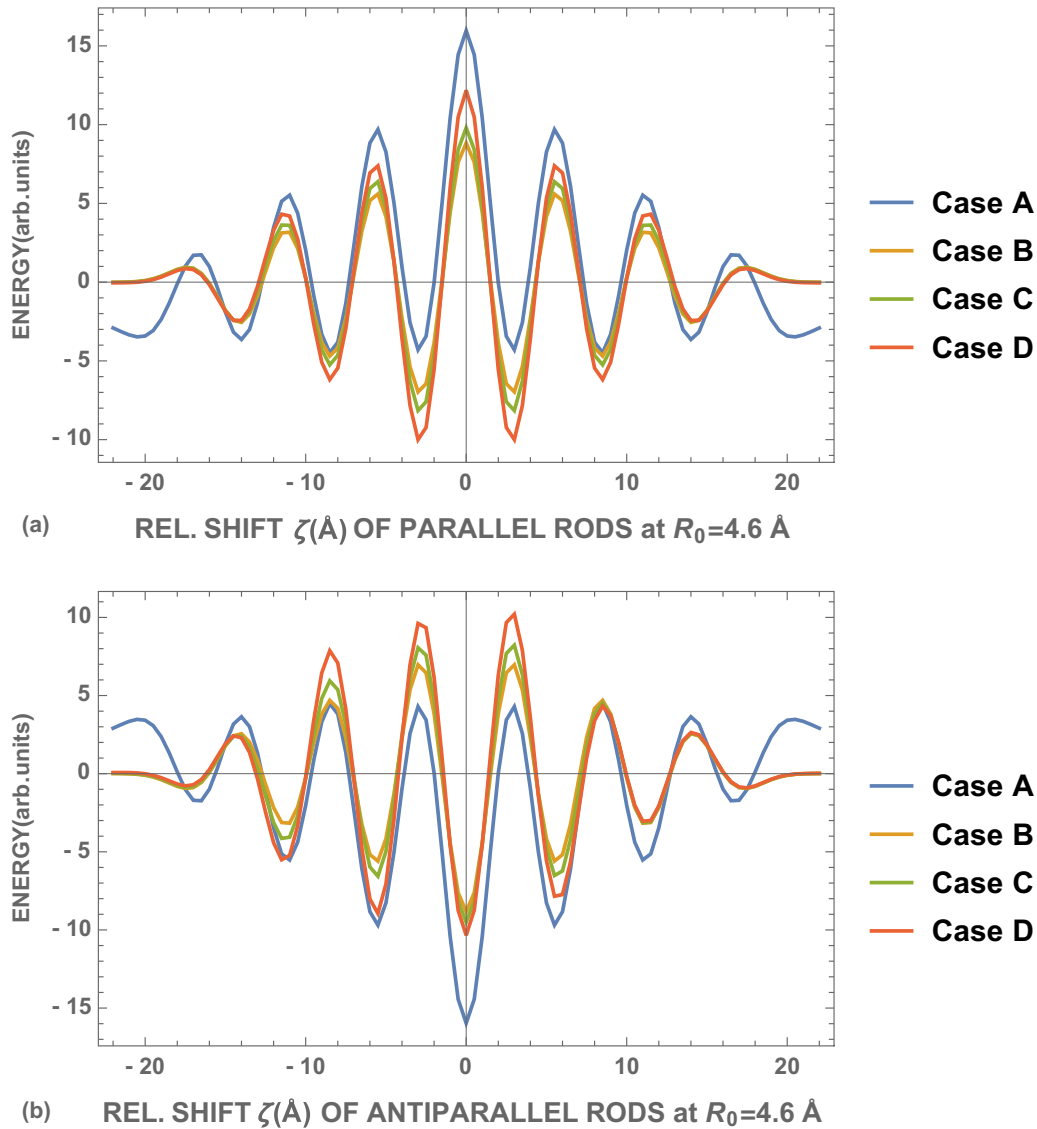
FIG. 6. The dependences of the electrostatic interaction energy between the rods separated by $R_0 = 4.6$ Å as functions of the relative shift ζ (21) along their axes as defined in Fig. 4. The four curves correspond to the charge density profiles shown in Fig. 5. Part (a) corresponds to parallel rods, and (b) corresponds to antiparallel rods. The cases A, B, C, and D correspond to the topmost to bottommost curves in the *minima* near $\zeta \approx 3$ Å in (a), and the bottommost to topmost curves in the *maxima* near $\zeta \approx 3$ Å in (b). Note the significant changes in the cases B, C, and D with respect to case A, which has all amplitudes equal. The numerical values of the energy shown in arbitrary units have to be multiplied by $7.19 \times 10^{-20} \sigma^2$, where σ is the actual amplitude in Coulomb/m^2 corresponding to the reference amplitude 1, as described in the text.

If the amplitudes of *only the end half-waves* ($s1$ and $s8$) are reduced to 0.4 (case B), the energy minimum of the AP structure *increases* to ~ -8 units, while that of the P structure is *lowered* to ~ -7 units. As the two minima are now much closer than in the case A, we can hope for the occurrence of the ferroelectric phase in this case.

We discuss the reason for this very useful change before we consider other cases C and D shown in Fig. 6. The mutual positions of the two rods corresponding to the energy minima in the P and AP structures are shown in Fig. 7.

R_0 is very small, and the interactions involving the charges belonging to the two *end half-waves* have a strong effect on the total energy in both P and AP structures. We note that in the P structure, the following three interactions of the bottommost half-waves with amplitude $s1$ make the *most important*

contributions to the energy of the pair: $-s1\,s2$ is the strongest interaction, and $+s1^2$, $+s1\,s3$ make significant contributions. There are similar contributions at the upper end as well. In the case of the AP structure, the important terms are as follows: $-s1\,s8$ (strongest), $+s1\,s7$, and $+s2\,s8$. When $s1$ and $s8$ are reduced to 0.4, the energy in the P case has the three contributions proportional to -0.4, $+0.16$, and $+0.4$, respectively. In the AP case, the contributions are -0.16, $+0.4$, and $+0.4$. Thus, for *parallel* rods, compared to case A of Fig. 6(a), while the decrease in the magnitude of the negative energy of case B is relatively small, the decrease in the positive energy is much larger. On the other hand, in the AP case, while the drop in the magnitude of the negative energy between case A and case B of Fig. 6(b) is large, the positive energies decrease by smaller magnitudes. This gives rise to the differences seen
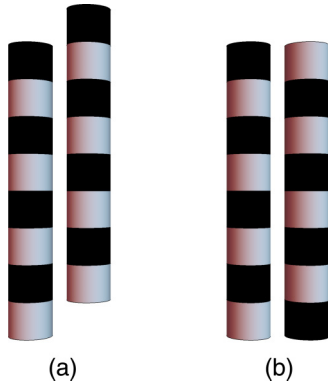
FIG. 7. Mutual positions of the two polar rods with the lowest electrostatic interaction energy for (a) parallel (P) and (b) antiparallel (AP) mutual orientations.

between the A and B cases shown in Figs. 6(a) and 6(b). The dependence of the lowest minimum energy at $\zeta(21) = 0$ of the AP structure on the inter-rod separation R_0 is shown in Fig. 8 for the case B, with only $s1 = s8 = 0.4$, and the amplitudes of all other charge waves equal to 1. As expected, the magnitude of the attractive energy *falls sharply* with R_0. At small R_0, parts of the surfaces of the two rods with charges of opposite signs *face each other* with a separation much smaller than R_0 (Fig. 7), contributing to the strong interaction. As R_0 is increased, this *gap* increases rapidly, giving rise to the steep variation in the interaction energy. As R_0 is increased beyond $\sim$10 Å, each rod experiences an *average* charge structure of the other rod, which looks like an *extended dipole*, and the energy falls off quite gently with R_0.

Another important feature to note is that when $s1 = s8 = 0$, the contributions from the *edge charges vanish*, and the relative enhancement of the energy of the parallel rods with respect to that of the AP rods seen in Fig. 6 also vanishes. The maximum advantage for the parallel rods is obtained for $s1 = s8 \approx 0.5$. All further calculations have been made for $s1 = s8 = 0.4$.

However, when only $s1$ and $s8$ are reduced, the relative enhancement of the P-type interaction is still not sufficient
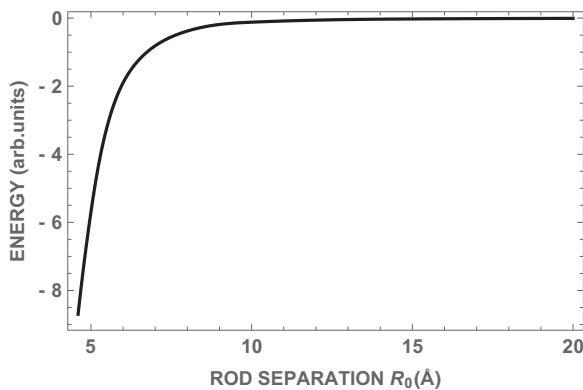

FIG. 8. Variation of the electrostatic energy between two antiparallel rods with the shift along Z fixed at $\zeta(21) = 0$ [as shown in Fig. 7(b)] and the charge structure as in case B of Fig. 5, as a function of the separation R_0 between the rods.

to give rise to the ferroelectric phase, as we will discuss in the next section. Thus, we have also shown in Figs 5(c) and 5(d) two more curves, with $s3 = s4 = 1.2$ in case C, and $s3 = s4 = 1.5$ in case D, apart from the reduced $s1 = s8 = 0.4$ as in case B. As the amplitude $s3 = s4$ is increased, the energy minima in both P and AP cases are lowered, but the difference in the P case is larger than that in the AP case. As electrostatic interactions from rods that are farther apart can also be expected to contribute to the stability of the phase, we show in Figs. 9(a) and 9(b) the $\zeta(21)$ dependences of the energy when $R_0 = 6$ Å, and in Figs. 10(a) and 10(b) for $R_0 = 10$ Å. When $R_0 = 6$ Å, in the AP case the lowest minimum at $\zeta(21) = 0$ hardly depends on the values of $s3 = s4$, and the second lowest minima at $\zeta(21) \approx \mp \lambda$ show the differences in the energies between the positive and negative values of $\zeta(21)$. In the P structure, the minimum is lowered for larger values of $s3 = s4$. In both P and AP cases, there is more than a threefold decrease in the minimum energy compared to the case with $R_0 = 4.6$ Å. When R_0 is increased to 10 Å, the minimum energy *decreases by about two orders* of magnitude compared to that for $R_0 = 4.6$ Å in both P and AP cases. The asymmetry between the dependences on $+\zeta(21)$ and $-\zeta(21)$ is much more obvious in the AP structure, which has a lower minimum compared to the P structure [Figs. 10(a) and 10(b)]. This shows that for small R_0 values like 4.6 Å, the interaction between two neighbors is very sensitive to the detailed structure of charge distribution as seen in Figs. 7(a) and 7(b). As the rods move farther apart, the contributions from the different parts of the rod are averaged out, and the rods experience an effective dipolar interaction.

In the condensed nematic phase, each rodlike molecule is surrounded by five or six near-neighbor rods. It is clear that in such a case, not all near neighbors can have the favored $\zeta(21)$ values as in Figs. 7(a) and 7(b). In the next section, we consider the electrostatic interaction in a cluster of rods that are organized in a structure that is *representative* of a condensed state.

III. AVERAGE ELECTROSTATIC ENERGY OF A ROD IN A SMALL CLUSTER

First, we consider a triplet of rods. All three molecules can be parallel as in Fig. 11(a). However, as is well known [1], in the AP case there is a *frustration* in the orientation of a *third polar rod* with respect to an antiparallel pair [Figs. 11(b) and 11(c)]. The calculations of the previous section show that with respect to a pair in a minimized energy structure with some $\zeta(21)$, the ζ-shift of the third rod may prefer a specific value to minimize the total energy of the triplet. The shift $\zeta(31)$ between the rods 1 and 3 is needed in calculating the interaction energy between them, and $\zeta(32) = \zeta(31) - \zeta(21)$ between 3 and 2 is used in calculating the corresponding energy. Interactions with a higher number of neighbors will influence the overall structure. For the sake of simplicity, we make the following approximations: (i) The axes of all the rods are perfectly aligned along the Z axis, i.e., the *apolar* nematic order parameter $\langle P_2(\cos\theta) \rangle = 1$. The ferroelectric to apolar nematic transition point is usually found to be well below the nematic-isotropic transition temperature [34,38,40] justifying this assumption. (ii) The circular *cross sections* of the rods
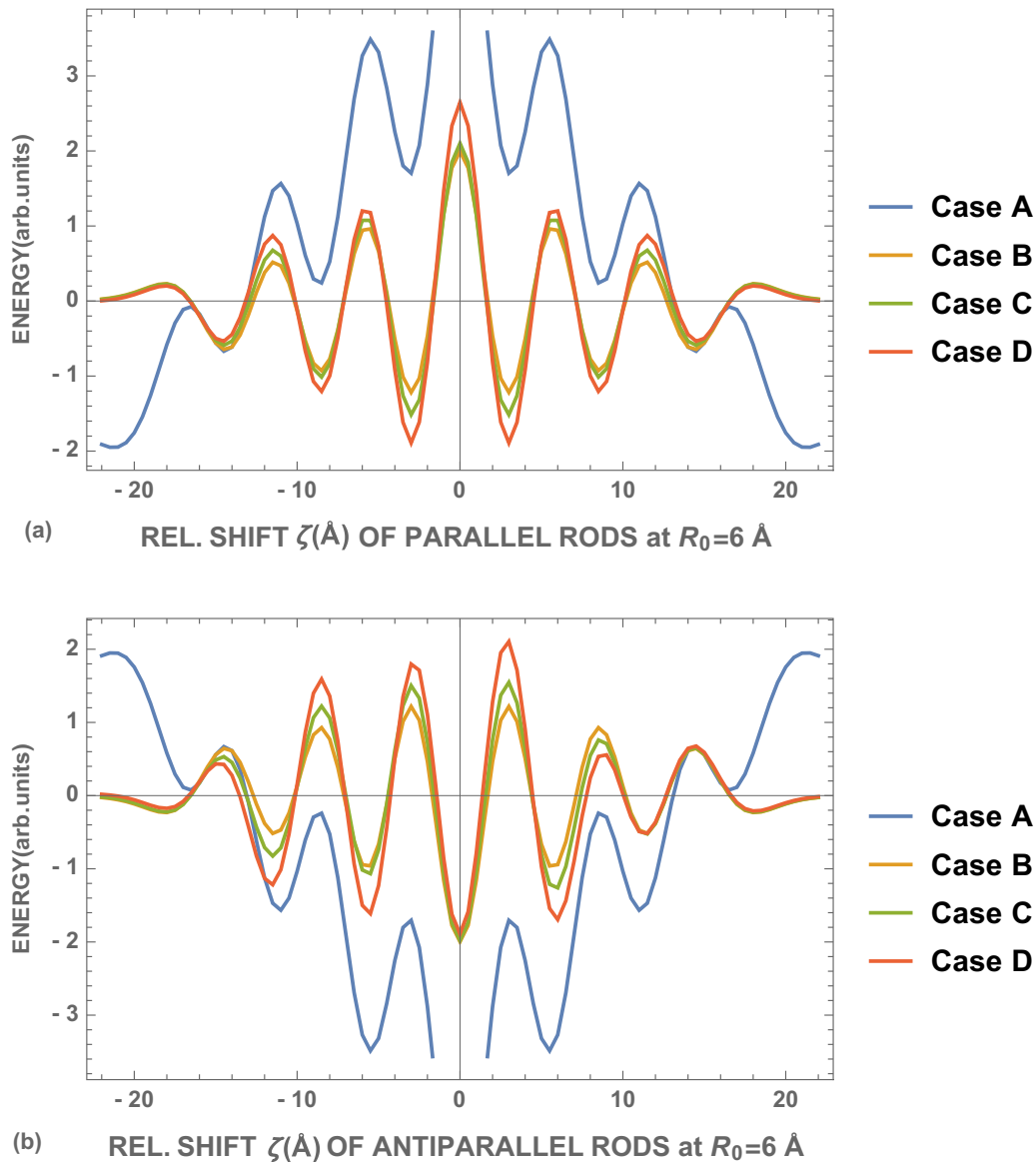
FIG. 9. Electrostatic interaction energy between two polar rods as a function of the mutual shift ζ (21) when the lateral separation $R_0 = 6$ Å for (a) parallel and (b) antiparallel rods. The minimum energies in both cases are about three times lower in magnitude compared to the case with $R_0 = 4.6$ Å. The ordering of the curves corresponding to the four cases is the same as in Figs. 6(a) and 6(b). The asymmetry between positive and negative shift ζ (21) in the AP structure for the B, C, and D cases can be noted.

are arranged in a hexagonal lattice in the *XY* plane (Fig. 12), though the rods *do not form layers* in either of the liquid crystal structures. Neighboring rods have an imbricated arrangement as shown in Fig. 11, and rods with maximal overlap with neighbors can be described to be in a *pseudolayer*. (iii) This implies that the distance between the axes of nearest neighbors is fixed at some value R_0 in the *XY* plane. An increase in R_0 reflects a lowering of the number density of molecules with an increase in temperature. (iv) As the inter-rod interaction energy falls off rapidly with R_0 (Figs. 6, 8, 9, and 10), we limit the calculation of the energy to a structure with a total of 19 rods in a pseudolayer, such that the interaction of the central rod with its second nearest neighbor is also taken into account (Fig. 12). (v) The rods in a given pseudolayer have overlaps with rods lying in neighboring pseudolayers above and below the given one along the *Z* axis. We include a second

set of 19 molecules lying in a pseudolayer with higher values of *Z* in the calculation of the total energy. We assume that due to the favorable electrostatic interaction, the positive end of the upper rod lies just above the negative end of the lower rod and vice versa, to form a chain along *Z*. Indeed, the x-ray studies on the compound RM734 (Fig. 2) have shown *three orders* of diffuse scattering corresponding to the length of the molecule *l* in both the apolar and ferroelectric nematic phases [33]. This implies that the *local structures* of the molecules are quite *well defined* in both apolar and polar nematic phases. Such end-to-end arrangements have also been found in the MD simulations [38,39] of RM734. We assume that even as R_0 increases with temperature, there is no change in the chain structure along the *Z* axis.

The hexagonal structure shown in Fig. 12 is made of the triplets of rods 1, 2, and 3 as displayed in Fig. 11. The 38 rods
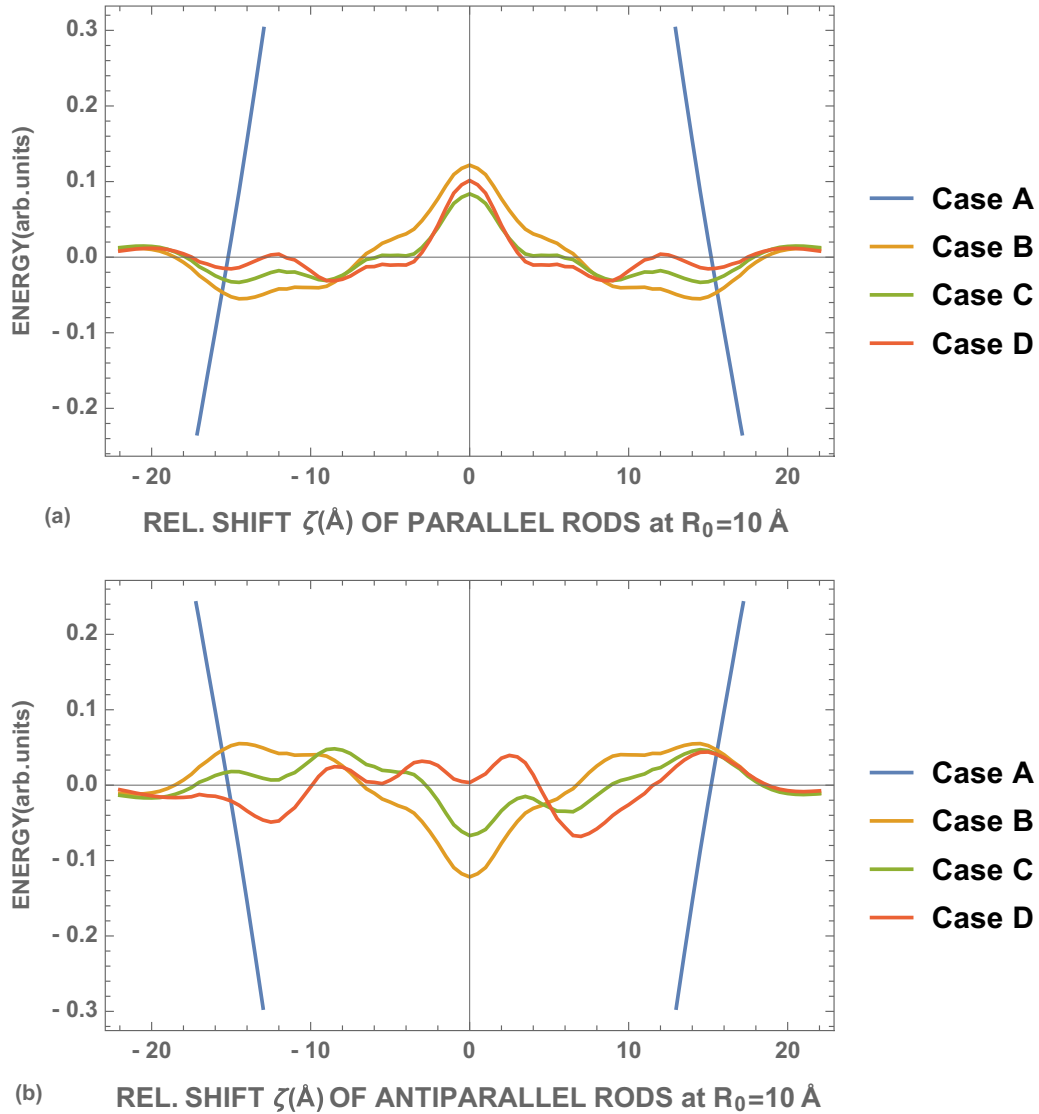
FIG. 10. Variation with relative shift of the electrostatic interaction energy between two rods with a lateral separation of 10 Å for (a) parallel and (b) antiparallel rods. The ordering of the curves corresponding to cases A, B, C, and D is the same as in Figs. 6(a) and 6(b). Note the steep reduction in the energy compared to the cases with $R_0 = 4.6$ Å, and the strong asymmetry between the dependences on $+\zeta(21)$ and $-\zeta(21)$ for the AP structure in cases C and D.

in the two overlying pseudolayers described above have a total of 703 inter-rod interactions, each of them to be calculated as described in Sec. II. Obviously, many of the interactions fall into equivalent groups, greatly reducing the total number of calculations. In the following section, we present the results of the calculations.

IV. RESULTS AND DISCUSSION

The total energy of the 38 rods is calculated by assuming reasonable values of $\zeta(21)$ and $\zeta(31)$ defined in Fig. 11, using the results of calculations of Sec. II. The two parameters are iteratively varied until the energy is minimized for the given value of R_0. In the antiparallel structure, the rods with labels 1 and 2 in Fig. 12 have opposite orientations, and the dipole moments are canceled. If all the rods labeled 3 as well as 3* in Fig. 12 are oriented along the same direction, an extended

medium will have a net polarization that is 1/3 of the polarization **P** exhibited by the ferroelectric phase, and corresponds to a ferrielectric structure. If, on the other hand, the orientations of the 3-type rods in successive rows, labeled as 3 and 3* in Fig. 12, have opposite orientations, as shown in Figs. 11(b) and 11(c), an extended sample will have 0 polarization. This structure can be designated as antiferroelectric structure. In this case, $\zeta(31)$ for 3-type rods is defined as in Fig. 11(b). From simple geometrical considerations, $\zeta(3*1)$ as defined in Fig. 11(c) has to be equated to $\zeta(32)$ corresponding to the 3 type rods of Fig. 11(b), and also $\zeta(3*2) = \zeta(32) + \zeta(21) = \zeta(31)$. This ensures that both rod 3 and rod 3* have similar overlaps with respect to both their parallel and antiparallel neighbors in calculating the total energy of the cluster.

Calculations of the *energy per rod* using the case B in Sec. II, with only $s1 = s8$ reduced to 0.4, and equating all other s-values to unity, shows that only the antiferroelectric
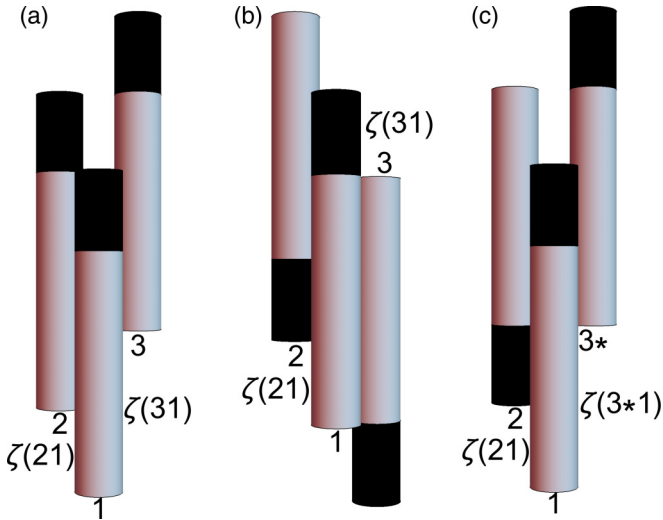
FIG. 11. Schematic figure showing triplets of polar rods, with *equal* lateral separation R_0 between each of the three pairs. The relative shifts $\zeta(21)$ and $\zeta(31)$ are those of rod 2 with respect to rod 1, and rod 3 with respect to rod 1, respectively. When rods 1 and 2 are antiparallel, (b) rod 3 can be parallel to rod 2 or (c) rod 3* can be parallel to rod 1.

phase is stable down to $R_0 = 4.6$ Å. The energy minimum has the lowest value for $\zeta(21) \approx 3.9$ Å and $\zeta(31) \approx 7.45$ Å for *parallel* rods, the actual ζ-values varying slightly with the values of $s3 = s4$ as well as R_0. For the *antiferroelectric* structure, $\zeta(21) \approx -0.85$ Å and $\zeta(31) \approx 6.55$ Å. If we now enhance $s3 = s4$ to 1.15, the antiferroelectric structure has a lower energy as R_0 is decreased only down to ~4.9 Å
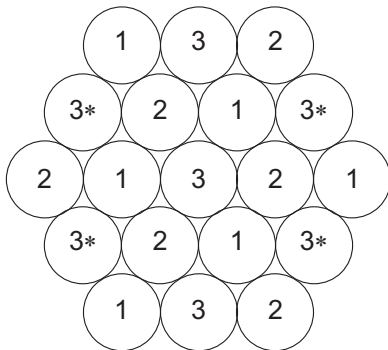

FIG. 12. Schematic diagram showing the assumed arrangement of the circular *cross sections* of the polar rods arranged in a hexagonal structure made of the triplets of molecules 1, 2, and 3 shown in Fig. 11. In the ferroelectric phase, all the polar rods have parallel orientations. When rods labeled 1 and 2 are antiparallel, rods labeled 3 can be parallel to rod 2, say, as in Fig. 11(b). If all of the rods 3 and 3* are parallel, the medium will have a net polarization **P**, which is 1/3 of the value in the ferroelectric phase, and corresponds to a ferrielectric phase. If rods 3 and 3* in alternating rows have opposite orientations [as in Figs. 11(b) and 11(c)], the net polarization of the medium is 0. The figure represents the *top view* of the assumed structure. The side view consists of a collection of triplets shown in Fig. 11, which do *not* form a smectic-like layer with all molecular centers in a plane.

TABLE I. Dependence of electrostatic energy (arb. units) per rod on R_0.

(a) $s1 = s8 = 0.4$, $s3 = s4 = 1.15$, $s2 = s5 = s6 = s7 = 1.0$			
R_0	E (Ferro)	E (Antiferro)	ΔE
4.7 Å	−7.471	−7.435	−0.036
4.8 Å	−6.652	−6.624	−0.028
4.85 Å	−6.278	−6.264	−0.014
4.9 Å	−5.913	−5.921	+0.008
4.95 Å	−5.591	−5.603	+0.012
5.0 Å	−5.280	−5.299	+0.019
5.1 Å	−4.691	−4.741	+0.050
(b) $s1 = s8 = 0.4$, $s3 = s4 = 1.20$, $s2 = s5 = s6 = s7 = 1.0$			
R_0	E (Ferro)	E (Antiferro)	ΔE
4.8 Å	−7.006	−6.839	−0.167
4.87 Å	−6.283	−6.198	−0.085
4.9 Å	−6.090	−6.010	−0.080
4.93 Å	−5.902	−5.842	−0.060
5.0 Å	−5.493	−5.469	−0.024
5.05 Å	−5.207	−5.195	−0.012
5.1 Å	−4.904	−4.907	+0.003
5.15 Å	−4.636	−4.652	+0.016
5.2 Å	−4.372	−4.405	+0.033

[Table I(a)]. For lower values of R_0, the ferroelectric structure has a lower energy. The crossover R_0 increases to ~5.1 Å if $s3 = s4$ is increased to 1.2 [Table I(b)], again with $s1 = s8 = 0.4$ as before. We have also found that the energy of the ferrielectric structure, with both rods labeled 3 and 3* in Fig. 12 having parallel orientations, is higher than those of both the ferroelectric and antiferroelectric structures when $s3 = s4 = 1.15$ at all the values of R_0 for which calculations have been made. As such, we compare only the energies of the ferroelectric and antiferroelectric structures. The difference in the energies, $\Delta E = E$ (Ferro) $- E$ (Antiferro), is shown in Fig. 13 for the two cases for which the relevant data are shown in Table I.

These calculations clearly show that the rods with the effective charge distributions along their lengths as described above can favorably form the ferroelectric phase with all rods aligned parallel to one another as the density increases beyond some reasonable value. The calculations have been made for a regular arrangement of the rods, with the axes of the rods being strictly parallel to one another [$\langle P_2(\cos\theta)\rangle = 1$]. The nematic is a three-dimensional fluid, and the structure is not rigid. The apolar order parameter is not fully saturated, and it can be expected to vary slightly with temperature. As such, our calculations are only *indicative* of the *structural features* of the molecules which are necessary for the occurrence of the ferroelectric nematic phase. Nevertheless, it is clear that the most important requirements are for the molecules to have (a) an *alternating* charge distribution along the length, produced either by ester linkage groups between the highly polarizable phenyl rings or fluorine side substitutions on the phenyl rings, (b) a *low* charge density near the *two ends*, which is ensured by having either NO_2 group or the three fluorine substitutions in ortho positions at one end and a short chain at the other (see
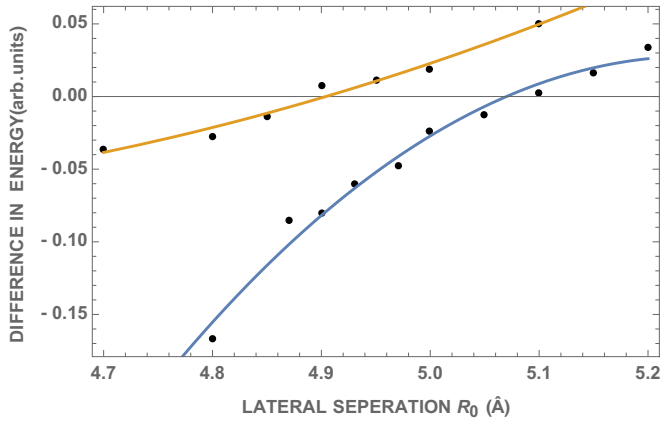
FIG. 13. Variations of the difference in the electrostatic energy per rod between the ferroelectric (F) and antiferroelectric (AF) structures as described in the text with the lateral separation R_0 between the rods. The F structure has lower energy compared to the AF structure below some value of R_0 (see Table I). The points are calculated values, and the lines are guides to the eye. The upper curve corresponds to $s3 = s4 = 1.15$, and the lower one to $s3 = s4 = 1.2$, with $s1 = s8 = 0.4$ in both cases. The crossover R_0 *increases* with the value of $s3 = s4$. It is clear that the actual amplitude of the charges of the molecule must be large enough for the difference in the energy to be larger than the thermal energy $k_B T$, which implies that the net longitudinal dipole moment must be large, as already noted in earlier models [20,24]. (The scatter in calculated energy differences arise from the errors in numerical results of the two energy minima, each of which is a summation over a large number of integrals.)

Fig. S20 of Ref. [38]), and (c) an enhanced charge density in the middle of the rod, like that generated by a side substitution of OC_nH_{2n+1} group with a small n, or the two oxygens of the dioxane group. Up to now, these requirements have been met by only the two basic structures shown in Fig. 2. Further, the absence of the ferroelectric phase if the NO_2 group is replaced by the CN group [39,40] also becomes clear as the latter will not give rise to the reduced charge density near the lateral periphery of the molecule. As described in the Introduction, the statistical mechanical theories developed to predict the FN phase [20,23,25,26] in systems of spheres or disks are based on the interactions between *point dipoles* usually fixed at the molecular centers. The interactions are *short-ranged* in a uniform FN, because of the mathematical nature of the dipolar interaction potential. Our calculations reveal that even in rigid rodlike molecules with a specific structure of the alternating charges, the FN is stabilized entirely by short-range interactions, such that the neighboring molecules are strongly influenced by the overlap of the structural features (Figs. 7 and 8). On the other hand, two rods even at about twice the separation R_0 of the nearest neighbors experience only an averaged dipolar interaction, which is highly reduced and actually favors an antiparallel orientation (Fig. 10). Thus, our calculations only on a cluster of 38 molecules can be expected to qualitatively reflect more elaborate calculations involving a larger number of molecules. The local structure which minimizes the energy is somewhat complex, with different values of $\zeta(21)$ and $\zeta(31)$ in both AF and F structures. Thus, a full-fledged statistical mechanical calculation, which has to take into account orientational and translational distributions about the short-range structure leading to the long-range polar order, can be expected to be quite involved and is beyond the scope of this paper. However, our calculations provide a *justification* for the *effective potential assumed* to favor polar order in the model proposed in Ref. [24], which leads to the isotropic-N-FN sequence as the density is increased.

Further, the experimental observations [34,38,40] as well as the calculations presented above indicate that in the bulk *liquid* medium, the relevant phase transition can be assumed to be that between paraelectric to ferroelectric phases. In view of the very high apolar order, the transition can be described by the Ising model, as noted in [38]. In this model, in the paraelectric phase the molecular dipoles are assumed to have equal probability of orienting either along the $+\mathbf{Z}$ or $-\mathbf{Z}$ direction, without considering any detailed local antiferroelectric arrangement described above. The electrostatic interaction energy of a given polar rod with only the z nearest-neighbor rods in the lattice is taken into account. The ferroelectric order parameter is just given by

$$\boldsymbol{m} = \hat{z}\frac{N_+ - N_-}{N_+ + N_-}, \tag{5}$$

where N_+ and N_- are the number of polar molecules in a unit volume aligned along the $+\mathbf{Z}$ axis and the $-\mathbf{Z}$ axis, respectively. In the mean-field approximation, the entropy of the medium for a given order parameter $\boldsymbol{m}$ can be calculated by counting the number of configurations with given values of N_+ and N_- [41]. This enumeration is easily made in the lattice-gas model [41] to calculate properties of the ferroelectric such as the temperature variation of the polarization $\mathbf{P}$. Very close to the transition point T^*, the relevant free energy reduces to the usual Landau expression with a temperature-dependent quadratic term and a temperature-independent quartic term in $\boldsymbol{m}$. This of course leads to only a second-order paraelectric to ferroelectric transition, while the experiments [34,38,40] point to a very weak first-order transition. This implies that a detailed model taking into account the coupling of $\boldsymbol{m}$ with other relevant variables is needed for a more realistic description of the transition. As seen in the calculations above, the ferroelectric order occurs when the inter-rod separation is reduced below some value, at which the electrostatic energy has a very steep variation with R_0 (Fig. 8). This means that the relevant order parameter $\boldsymbol{m}$ is coupled to the *density* of the medium. Density measurements in RM734 and RM734CN have shown that in the former case, the *density* gets *enhanced* at lower temperatures compared to that in the latter, which does not exhibit the ferroelectric phase [39]. Furthermore, in general one can expect that an increase in density should also increase the apolar order parameter $\langle P_2(\cos\theta)\rangle$. Indeed, this was seen as an enhanced birefringence in the ferroelectric phase of RM734 in Ref. [38]. The coupling with the density is clearly the primary effect. We write the free-energy density near the phase-transition temperature as

$$F_c = \frac{a}{2}(T - T^*)m^2 + \frac{b}{4}m^4 - cm^2\delta\omega + \frac{d}{2}\delta\omega^2, \tag{6}$$

in which $\delta\omega$ is the *excess* density above the equilibrium value in the absence of the coupling, and m is the magnitude of $\boldsymbol{m}$. The coupling (with constant $c > 0$) lowers the free energy,

while the deviation costs a positive energy which depends quadratically on the deviation. Minimizing the free energy with respect to the deviation yields $\delta\omega = (cm^2)/d$. Using this in Eq. (6), the free energy is now written as

$$F_c = \frac{a}{2}(T - T^*)m^2 + \left(\frac{b}{4} - \frac{c^2}{2d^2}\right)m^4 + \frac{g}{6}m^6. \quad (7)$$

The coefficient of the quartic term is clearly reduced due to the coupling between m and $\delta\omega$. If the coupling coefficient c is strong, the quartic term can even become negative, necessitating the sixth-order term to ensure stability of the ferroelectric phase. In this case, the transition becomes first-ordered in nature. This is the likely origin of the weak first-order paraelectric-to-ferroelectric transition reported in several compounds [34,38,40]. It may also be noted that the temperature dependence of the order parameter m close to T^* can be used to test if this is the physical mechanism. If the quartic term can be made to approach 0 by using suitable mixtures, the transition approaches a tricritical point, at which $m \propto (T^* - T)^{0.25}$, rather than the square root dependence predicted when the quartic term has a large enough positive coefficient [1].

Interestingly, a couple of weeks after the paper was originally submitted, the results on another compound modified from RM734 by substituting a fluorine atom in position R_3 while retaining $R_1 = CH_3$ and $R_2 = OCH_3$ in Fig. 2(a) were published [42]. Three distinct ferroelectric phases were found below the range of stability of the apolar N phase. As the temperature was lowered, polarization increased to about $6.9\ \mu C/cm^2$. In planar cells, the higher-temperature ferrophase exhibited wide domains, separated by relatively thick ($\sim 10\ \mu m$) walls, indicating Néel-type walls described in [40]. The rotational viscosity increased relatively rapidly as the temperature was reduced in the two lower-temperature ferrophases. The *density* has a remarkable *increase* of $\sim 10\%$ as the temperature is lowered in the ferrolectric liquid-crystal range. The authors suggest that *increased short-range ordered spatial correlation between the long axes of the molecules which may have hexagonal structure* generates the three ferrophases. It appears that the additional F atom modifies the electrical structure of the molecule sufficiently, and generates a *variable wavelength* in the charge oscillations along the length of the molecule. This could give rise to different short-range structures, and the energy minima can shift from one to the other as the temperature is varied.

Our main purpose in this work is to identify the *molecular features* for the occurrence of the FN phase as a low-temperature phase in some highly polar compounds with restricted structural parameters of the rodlike molecules. We note that both measurements of the reduction of the splay elastic constant as the transition is approached from higher temperatures [35,36], and observations of stripes [36,40] as well as enhancements in the dielectric constant and SHG signal in that temperature range, have been interpreted as arising from a splay nematic phase [35,36,40], the theory of which has been refined recently [43,44]. From our calculations, it is clear that as the energy difference between the AP and P structures is reduced (Fig. 13), fluctuations with the polar order will arise in the higher-temperature phase, as in any

weak phase transition [41]. As discussed in Refs. [36,37], a coupling of such supramolecular polar structures with the flexopolarization due to splay distortion reduces the effective splay elastic constant, and can give rise to the periodic splay modulation. However, the polarization *within* the *ferroelectric* phase is extremely large, and the polarization charges due to splay distortion generate a prohibitively large positive energy [38]. As such, these periodic "splay domains" can be expected to simply go over to domains with opposite orientations of undistorted **P** as in any typical ferroelectric material. Depending on the sample, the walls between these domains can be extremely narrow, as the **P** vector can flip over molecular dimensions in the FN phase [38], or relatively thick with a bend distortion of the **P** vector [40,42].

V. CONCLUSIONS

Though predicted as the mechanism responsible for the *orientational* order of nematic liquid crystals made of rod-like molecules over a century ago [2], the polar interaction leading to ferroelectric nematic turned out to be quite elusive until very recently [34,38]. The main reason is of course the preferential antiparallel near-neighbor orientation to minimize the electrostatic energy in simple rodlike molecules with a strong longitudinal dipole at one end, and an alkyl or alkoxy chain with several carbon atoms at the other end [8]. This in turn leads to a variety of unusual phenomena, suchas reentrance of the nematic, which requires further subtle balance in intermolecular interactions [15]. The ferroelectric nematic was found some time ago in polymeric molecules in which the longitudinal components of the monomer dipole moments add up, resulting in a very large value in each polymer chain [28]. The polymers cannot be switched easily due to high viscosity. The ferroelectric nematic has been discovered with *small rodlike* molecules with highly *restricted structures* [34,38,40]. It is not enough if the molecules have a large (~ 10 D) dipole moment, as was predicted by some theories [20]. Thus, if the end polar group NO_2 is replaced by CN in RM734 [Fig. 2(a)], the ferroelectric phase disappears. The *chain length* should be *very short*, and the molecular structure should incorporate a *few dipolar groups* attached to (like F substitution) or between (like ester groups) phenyl rings. The basic question is why the molecules with the restricted structures change over to the parallel rather than remaining with antiparallel order as the temperature is lowered below some value.

We have developed a model by noting that, as the molecules freely rotate, they can be represented by cylindrical rods with a longitudinal wave of *surface charge densities*. The inter-rod electrostatic interaction still favors antiparallel orientation if the amplitudes of all four waves are equal, even when the separation between them is very small. However, if the amplitudes of only the two *end half-waves* are *reduced*, the electrostatic interaction of antiparallel rods with full overlap is considerably lowered, while that of the parallel rods with appropriately shifted molecules is enhanced. This makes the two interactions comparable if the inter-rod separation is small, and each rod can experience the *spatial electrical structure* of the neighboring rod, as the gap between their surfaces is

very narrow. This is consistent with the experimental observation of the NO_2 end group favoring the ferroelectric phase, unlike the CN group. We have presented calculations on a cluster made of two pseudolayers with 38 rods, with their circular cross sections arranged in a hexagonal lattice in the plane perpendicular to the rods. Using an additional slightly enhanced amplitude in one interior surface wave, the electrostatic energy per rod actually favors parallel arrangement in the cluster compared to the fully antiferroelectric order when the lateral inter-rod separation is reduced below some value. The favorable interaction is highly short-ranged, and essentially restricted to nearest neighbors. The ferroelectric order builds up in the entire sample only when the density is high, and the near neighbors arrange themselves in a short-range structure with appropriate values of the relative shifts $\zeta(21)$ and $\zeta(31)$, such that the energy of ferroelectric order is optimized. The *short-range* nature of dipolar interaction in a ferroelectric nematic has been noted in some earlier theoretical studies [20,23,26]. The favorable ferroelectric interaction found in our model provides a justification for the *assumption* made in [24] to predict the occurrence of ferronematic phase in polar rods at high enough densities. In view of the very high nematic order, this changeover can be described by an Ising model, which reduces to the usual Landau theory close to the paraelectric-to-ferroelectric transition. We have also suggested that the weakly first-order transition found in all the cases can arise from the strong coupling between the polar order and the density of the medium. The density dependence is implied by our calculations (Figs. 8 and 13), as well as the difference in the experimental variations of the density in RM734, which forms the ferroelectric nematic, and RM734-CN, which does not [39]. Our calculations also offer a plausible explanation of the rather restricted structural features which are found in compounds exhibiting the FN phase. The molecules must have a few polar groups with lateral components of dipoles, like the ester linkage group and/or fluorine substitutions on the phenyl rings. As the molecules rotate freely, this can be represented by rods with longitudinal surface charge density waves. The two *ends* which have opposite charges must have lower amplitudes of the charge density, which is possible with the NO_2 group of RN734 (see Fig. S20 of Ref. [32]) or the three fluorine substituents on the end phenyl ring as shown in Fig. 2(b). The other end can have a *short chain*, with fewer than three carbon atoms, so that the charge density is reduced. The chain length cannot be long, as it is clear from Fig. 11 that both the parallel and antiparallel near-neighbor overlaps will not be conductive with long chains for the formation of structures that can have a long-range propagation. As such, longer chains can give rise to the well-known antiparallel structure with partial bilayer short-range order [9]. If the chain length is too long, the smectic phase is favored [1]. These considerations and the usefulness of additional laterally projecting dipoles in the interior of the rod in favoring the ferroelectric order are satisfied by all the compounds that have been found to exhibit the FN phase. Hopefully, synthetic chemists can design new compounds keeping these requirements in mind. We may also note that the FN phase found in the small rodlike molecules [34,38,40] is different from the one proposed by Born [2], whose model implies that the orientational order itself arises from the nonzero $\langle P_1(\cos\theta)\rangle$ order parameter. The experiments as well as the model presented in this paper imply that as in all other nematogens, the orientational order arises due to excluded volume and anisotropic dispersion interactions, and the ferroelectric order emerges only in a small number of highly polar molecules with specific spatial structural features of the molecules as the intermolecular separation is reduced at low enough temperatures.

[1] P. G.deGennes and J. Prost, *The Physics of Liquid Crystals* (Clarendon, Oxford, 1993).

[2] M. Born, Sitzungsber. Preuss. Akad. Wiss. **30**, 614 (1916).

[3] J. Valasek, Phys. Rev. **17**, 475 (1921).

[4] L. Onsager, Ann. N.Y. Acad. Sci. **51**, 627 (1949).

[5] W. Maier and A. Saupe, Z. Naturforsch. **13**, 564 (1958).

[6] For a review, see N. V. Madhusudana, in *Applications of Liquid Crystals*, edited by B. Bahadur (World Scientific, Singapore, 1990), Vol. 1, Chap. 2, p. 37.

[7] G. W. Gray, K. J. Harrison, and J. A. Nash, Electron. Lett. **9**, 130 (1973).

[8] N. V. Madhusudana and S. Chandrasekhar, in *Proceedings of the International Liquid Crystals Conference, Bangalore, 1973* [Pramana Suppl. I, 57 (1975)].

[9] A. J. Leadbetter, R. M. Richardson, and C. N. Colling, J. Phys. **36**, C1-37 (1975).

[10] P. E. Cladis, Phys. Rev. Lett. **35**, 48 (1975).

[11] N. V. Madhusudana, B. K. Sadashiva, and K. P. L. Moodithaya, Curr. Sci. **48**, 613 (1979).

[12] F. Hardouin, G. Sigaud, M. F. Achard, and H. Gasparoux, Solid State Commun. **30**, 265 (1979).

[13] G. Sigaud, F. Hardouin, M. Achard, and H. Gasparoux, J. Phys. **40**, C3-356 (1979).

[14] A. N. Berker and J. S. Walker, Phys. Rev. Lett. **47**, 1469 (1981).

[15] N. V. Madhusudana and J. Rajan, Liq. Cryst. **7**, 31 (1990).

[16] A. S. Govind and N. V. Madhusudana, Liq. Cryst. **14**, 1539 (1993).

[17] G. Nounesis, S. Kumar, S. Pfeiffer, R. Shashidhar, and C. W. Garland, Phys. Rev. Lett. **73**, 565 (1994).

[18] S. R.Warrier, D. Vijayaraghavan, and N. V. Madhusudana, Europhys. Lett. **44**, 296 (1998).

[19] G. Basappa and N. V. Madhusudana, Eur. Phys. J. B **1**, 179 (1998).

[20] F. Bisi, A. M. Sonnet, and E. G. Virga, Phys. Rev. E **82**, 041709 (2010).

[21] J. J. Weis, D. Levesque, and G. J. Zarragoicoechea, Phys. Rev. Lett. **69**, 913 (1992).

[22] D. Wei and G. N. Patey, Phys. Rev. A **46**, 7783 (1992).

[23] D. Levesque, J. J. Weis, and G. J. Zarragoicoechea, Phys. Rev. E **47**, 496 (1993).

[24] J. Lee and S. D. Lee, Mol. Cryst. Liq. Cryst. **254**, 395 (1994).

[25] P. Palffy-Muhoray, M. A. Lee, and R. G. Petschek, Phys. Rev. Lett. **60**, 2303 (1988).

[26] M. A. Osipov, P. I. C. Teixeira, and M. M. Telo de Gama, J. Phys. A **30**, 1953 (1997).

[27] E. M. Terentjev, M. A. Osipov, and T. J. Sluckin, J. Phys. A **27**, 7047 (1994).

[28] T. Furukawa *et al.*, Mol. Cryst. Liq. Cryst. **299**, 105 (1997).

[29] B. K. Sadashiva, R. Amaranatha Reddy, R. Pratibha, and N. V. Madhusudana, Chem. Commun. 2140 (2001).

[30] R. Amaranatha Reddy *et al.*, Science **332**, 72 (2011).

[31] M. A. Osipov and G. Pajak, Eur. Phys. J. E **37**, 79 (2014).

[32] R. J. Mandle, S. J. Cowling, and J. W. Goodby, Chem. Eur. J. **23**, 14554 (2017).

[33] R. J. Mandle, S. J. Cowling, and J. W. Goodby, Phys. Chem. Chem. Phys. **19**, 11429 (2017).

[34] H. Nishikawa *et al.*, Adv. Mater. **29**, 1702354 (2017).

[35] A. Mertelj, L. Cmok, N. Sebastian, R. J. Mandle, R. R. Parker, A. C. Whitwood, J. W. Goodby, and M. Copic, Phys. Rev. X **8**, 041025 (2018).

[36] N. Sebastian, L. Cmok, R. J. Mandle, M. R. de la Fuente, I. Drevensek Olenik, M. Copic, and A. Mertelj, Phys. Rev. Lett. **124**, 037801 (2020).

[37] S. Dhakal and J. V. Selinger, Phys. Rev. E **81**, 031704 (2010).

[38] X. Chen *et al.*, Proc. Natl. Acad. Sci. U.S.A. **117**, 14021 (2020).

[39] R. J. Mandle, N. Sebastian, and J. Martinez-Perdiguero, arXiv:2100.02722.

[40] J. Li *et al.*, Sci. Adv. **7**, eabf5047 (2021).

[41] P. M. Chaikin and T. C. Lubensky, *Principles of Condensed Matter Physics* (Cambridge University Press, Cambridge, 1995).

[42] R. Saha *et al.*, arXiv:2104.06520.

[43] M. P. Rosseto and J. V. Selinger, Phys. Rev. E **101**, 052707 (2020).

[44] E. I. Kats, Phys. Rev. E **103**, 012704 (2021).